JOURNAL OF MATERIALS SCIENCE 22 (1987) 887–895

Oxide-dispersed titanium alloys Ti–Y prepared with the rotating electrode process

S. NAKA, M. MARTY, H. OCTOR
Office National d'Etudes et de Recherches Aérospatiales, BP 72, 92322 Châtillon, France

This work deals with an evaluation of the range of cooling rates during solidification necessary to obtain rare earth oxide-dispersed titanium alloys, which constitute a potentially interesting alloy system for high temperature use, due to the thermodynamic stability of rare earth oxides in titanium. The results of the microstructural studies on binary Ti–Y alloy powders prepared by the rotating electrode process show that it is possible to obtain a fine and homogeneous dispersion of yttrium oxide Y_2O_3 in a titanium matrix with relatively moderate cooling rates ($\sim 10^4$ K sec^{-1}). The results also indicate that the stability of the dispersion is excellent during hot consolidation but only in the α phase temperature region (< 882.5° C). The preliminary mechanical tests performed on consolidated products show a substantial increase in 0.2% proof stress (about 100 MPa) up to 550° C with respect to unalloyed titanium of commercial purity. Above 550° C, this strength increment becomes negligible or disappears. These results imply that the oxide dispersion loses its hardening effect at high temperatures, probably due to the increasing importance of grain-boundary sliding.

1. Introduction

It is now expected that the requirements for titanium alloys with higher mechanical strength may be satisfied through rapid solidification processing. One alloy system to which much attention has been paid in the last few years for use at still higher temperatures is the titanium–rare earth system with a view to forming a dispersion of *in situ* oxidized rare earth particles [1–6]. This approach is based on the thermodynamic stability of rare earth oxides, which presumably reduces the rate of dispersion coarsening during high-temperature consolidation.

This study is aimed at determining the range of cooling rates during solidification and the type of rapid solidification equipment, necessary for obtaining the desired microstructure. With this objective, powder particles of binary Ti–Y alloys prepared with the rotating electrode process (REP) were microscopically examined in order to correlate the dispersion parameters (dispersed particle size and interparticle spacing) with the powder particle size.

In this paper, the results of various microstructural studies and of the mechanical tests conducted on consolidated products will be presented and discussed.

2. Experimental procedure

Ti–Y (1.84 wt % Y and 0.74 wt % Y) alloy ingots were prepared by arc-melting from T40 (Cezus) grade titanium and 99.9% pure yttrium (Johnson Matthey). Yttrium was selected as alloying element in this study; according to the thermodynamic data, yttrium oxide is one of the most stable rare earth oxides [7]. According to Sastry and co-workers [1, 2], yttrium is one of the most appropriate elements for a fine oxide dispersion in titanium.

The alloy ingots were forged at 850° C to 50 mm diameter rods, then several electrodes for REP atomization were prepared by machining from each of these rods.

Powders were produced by REP under an inert gas atmosphere with the following operative conditions:

nature of atmosphere: Ar–He mixed at 50–50;
electrode diameter: 41 mm;
rotation rate: 17 100 r.p.m.

The particle size distribution of the powders obtained with these conditions was determined by sieving (Fig. 1). Chemical analyses of raw T40 grade titanium, alloy ingots and as-solidified powder particles showed no significant difference in oxygen concentration level (~ 0.12 wt %).

Consolidation of alloy powders was carried out by hot isostatic pressing (HIP) or by extrusion. The operative conditions for HIP were as follows:

pressure: 1000 to 2000 bar (100 to 200 MPa);
temperature: 800 to 920° C;
hold-time: 3 h.

Microstructural examinations were carried out on powder particles as well as on consolidated products. Finally, some mechanical tests on consolidated products were carried out at 25, 300, 525 and 700° C.

3. Microstructural examinations

3.1. Arc-melted alloy

Fig. 2 shows a strong tendency of yttrium to segregate on the optical microscopy scale in the as-cast Ti–1.84% Y alloy electrodes. Electron diffraction analyses of this segregation on thin foils indicated that it was of yttrium sesqui-oxide, Y_2O_3 (Fig. 3). This

0022–2461/87 $03.00 + .12 © *1987 Chapman and Hall Ltd.*

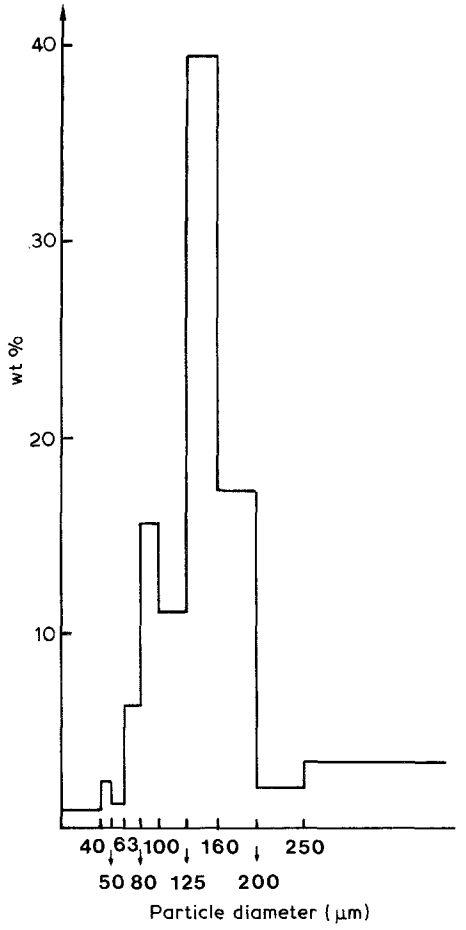

Figure 1 Particle size distribution of REP-produced powder of Ti–1.84 % Y.

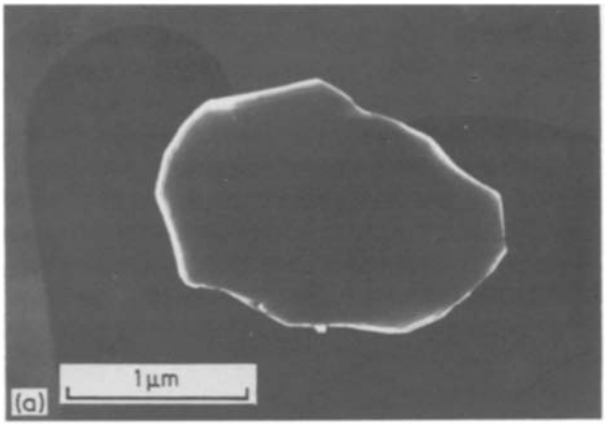

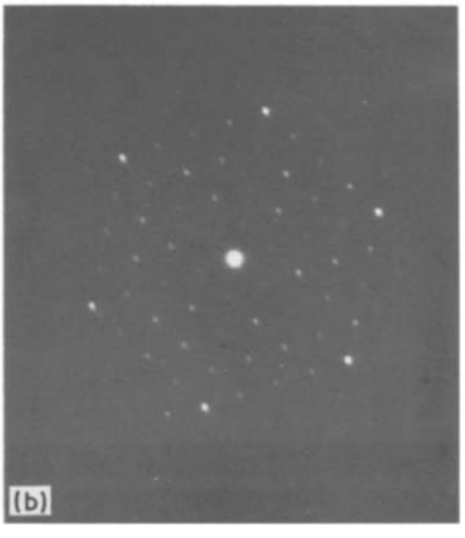

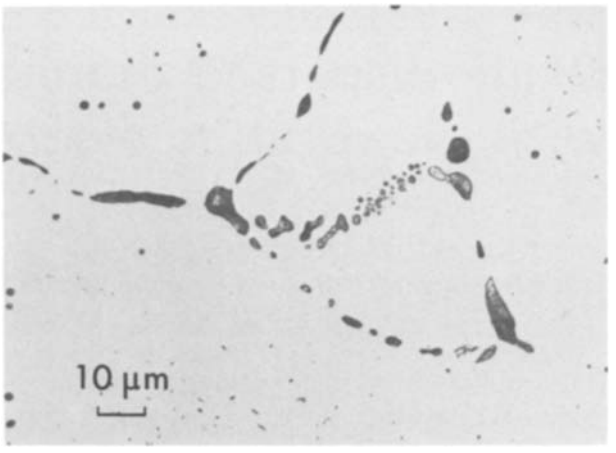

Figure 2 Important segregation of yttrium in the as-cast Ti–1.84 % Y alloy electrodes before REP atomization.

oxide possesses the bcc structure with $a = 1.06\,\text{nm}$ [7].

In a small ingot ($\sim 180\,\text{g}$) prepared also by arc-melting, the segregation observed by optical microscopy was as strong as in the alloy electrodes for REP atomization, but on thin foils of this ingot, a fine and rather homogeneous precipitation of Y_2O_3 was sometimes observed in a very localized manner (Fig. 4). This observation was a little surprising and we wondered whether a fine and very homogeneous dispersion could be obtained in this alloy system with a relatively moderate solidification rate. It is worth noting that such an observation was also reported by Konitzer *et al.* [3].

3.2. Powder particles

Scanning electron microscopy on the surface of powder particles (Fig. 5) revealed a dendritic structure. The electron back-scattering contrast due to the difference of atomic number between titanium and yttrium indicates a tendency of yttrium to form an interdendritic segregation on a powder-particle scale. The secondary dendrite arm spacing varies, at a rough estimation carried out on some powder particles, from 1 μm for particles of diameter $\phi < 40\,\mu\text{m}$ to $2.5\,\mu\text{m}$ for those of $125 < \phi < 160\,\mu\text{m}$.

Figure 3 Yttrium oxide precipitate in the as-cast Ti–1.84 % Y alloy electrodes: (a) dark-field image; (b) selected-area diffraction pattern of [1 1 1] pole; (c) schematic diagram of diffraction. (⊙) intense reflections, (●) weak reflections, (x) forbidden or very weak reflections.

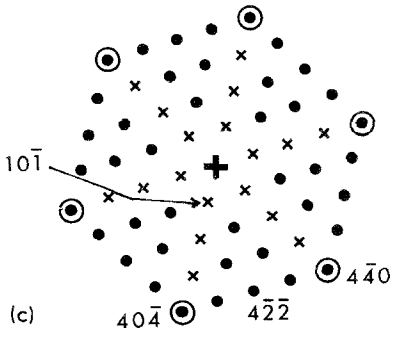

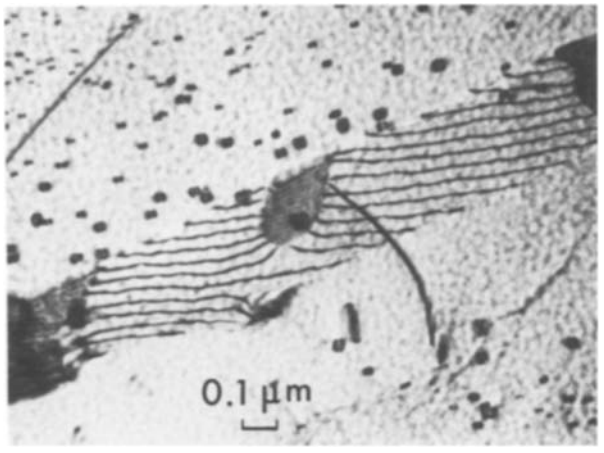

Figure 4 Fine and rather homogeneous precipitation observed in a very localized manner in an arc-melted small Ti–1.84 % Y alloy ingot.

Transmission electron microscopy performed on thin foils of some individual powder particles of $\phi < 40\,\mu m$ showed a fine and homogeneous dispersion, as shown in Fig. 6. This microstructure was not however observed systematically in all the powder particles (only in three powder particles among eight examined). Because of the difficulty in thin foil preparation, powder particles of other sizes could not be examined up to now.

3.3. Consolidated products

3.3.1. Fine and homogeneous oxide dispersion

In the products (Ti–1.84% Y) consolidated by HIP at 800° C, transmission electron microscopy revealed a fine and homogeneous dispersion for any initial powder particle size below 250 µm (Fig. 7). It must be noticed however that there are two populations of dispersed precipitates: a first population of very densely distributed small precipitates, and a second population, much less dense, of coarse precipitates.

3.3.1.1. First population: small precipitates. Bright-field images of these precipitates show a contrast due to the lattice distortion of the matrix around them (Fig. 8a), indicating that they probably possess a lattice coherency with the titanium matrix. An assessment of the size of these precipitates was therefore made with dark-field images (Fig. 8b); most of them possessed a size of 30 nm or below. Electron diffraction analyses indicated that these fine precipitates were of bcc yttrium oxide, Y_2O_3, and that they possessed an orientation relationship with the matrix: $\{1\,1\,1\}_{Y_2O_3} \| (0\,0\,0\,1)_{Ti}$ and $\langle 1\,\bar{1}\,0 \rangle_{Y_2O_3} \| \langle 1\,1\,\bar{2}\,0 \rangle_{Ti}$. This result is obvious on the selected-area diffraction pattern (Fig. 9) where the incident beam direction is parallel to $[1\,0\,\bar{1}\,0]$ of titanium and to $[1\,\bar{2}\,1]$ of Y_2O_3. Indeed the $4\,0\,\bar{4}$ reflection from Y_2O_3 lies along the $1\,\bar{2}\,1\,0$ systematic row of titanium and the $2\,2\,2$ reflection along the $0\,0\,0\,2$ systematic row. This orientation relationship must give two variants. This was confirmed by the position of the $2\,\bar{2}\,2$ reflection on two diffraction patterns of Fig. 10, obtained from two selected areas slightly apart one from another in the same matrix grain.

3.3.1.2. Second population: coarse precipitates. Contrary to the small precipitates of the first population, these coarse precipitates showed no lattice distortion

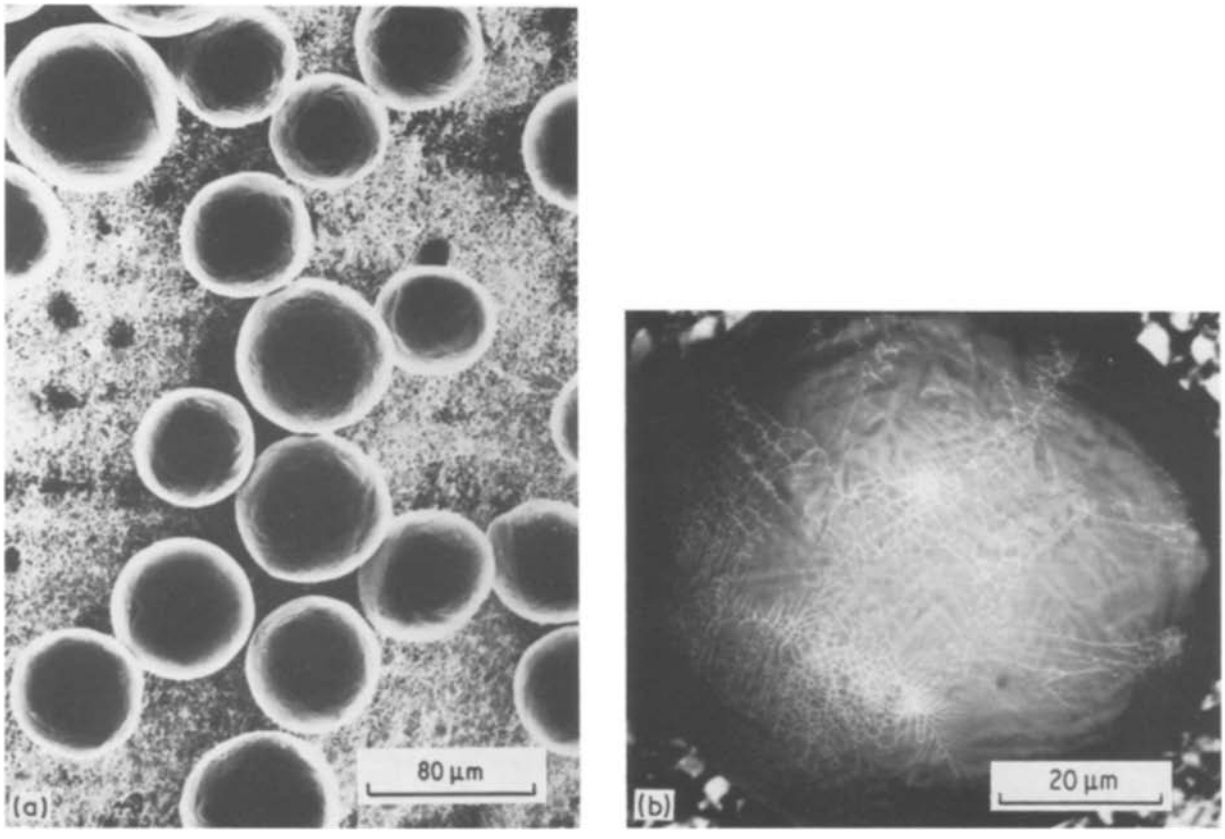

Figure 5 Scanning electron microscopy on the surface of powder particles: (a) powder particles ($63 < \phi < 80\,\mu m$); (b) dendritic structure revealed by electron back-scattering contrast.

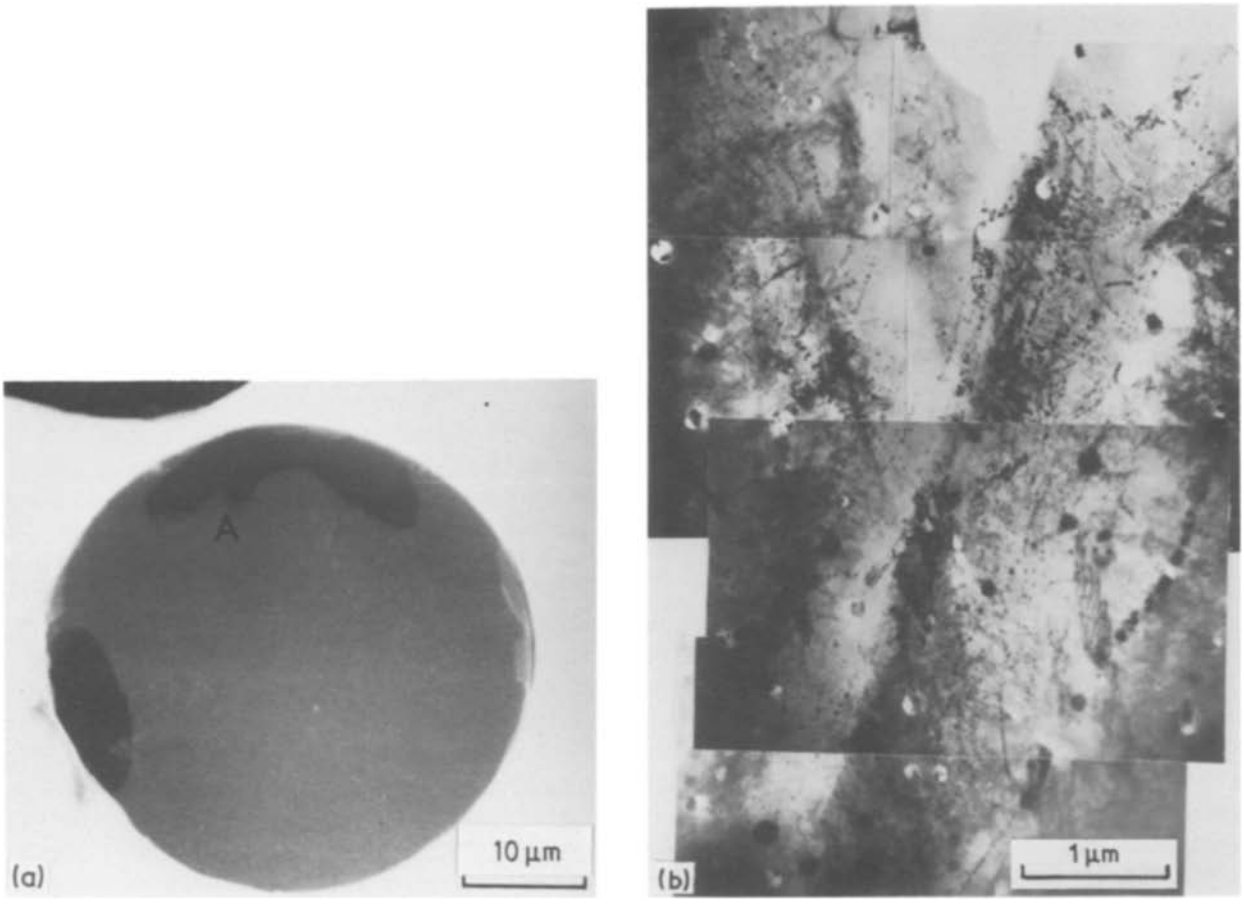

Figure 6 Transmission electron microscopy on individual powder particles: (a) thin foil of a powder particle of Ti–1.84 % Y embedded in gold; (b) microstructure observed in the area A of the thin foil.

contrast around them. Their size was larger than 0.1 μm and varied strongly, reaching sometimes up to 1 μm, but rarely above. Electron diffraction studies indicated that the precipitates of this population possessed the same crystal structure with the same lattice parameter as those of the first population. It suggests that these coarse precipitates are also of Y_2O_3 (Fig. 11). No particular orientation relationship was found between these precipitates and the matrix.

3.3.1.3. Influence of yttrium content and of consolidation temperature. The results of the observation of the Ti–1.84% Y alloy consolidated at 800° C are also valid for Ti–0.74 % Y.

The consolidation temperature may seriously modify the feature of dispersion. Indeed, whereas the products consolidated at 850° C presented a microstructure nearly identical (Fig. 12a) to that observed after HIP at 800° C, the first population of small precipitates disappeared completely for the benefit of the second population in the products consolidated at 920° C (Fig. 12b). This result indicates that the coarsening of yttrium oxide particles in a titanium matrix is suddenly accelerated when the matrix phase changes from α to β.

4. Mechanical properties

The results of the preliminary mechanical tests carried out on products consolidated at 800° C by HIP or by extrusion from powder particles of 125 to 160 μm in diameter are presented in Fig. 13. This figure includes, for a comparison, the results obtained by Sastry *et al.* [2] on the Ti–1.0 % Er alloy elaborated using an electron-beam melting and splat quenching apparatus.

This figure indicates in the first place a substantial increase in 0.2% proof stress (about 100 MPa) compared to pure titanium up to 550° C. In this temperature range, moreover, the 0.2% proof stress of products consolidated by extrusion is slightly higher than that of products subjected to HIP. At temperatures higher than 550° C, the increment in 0.2% proof stress falls and becomes almost negligible at 700° C, while a sudden increase in total elongation during the tensile tests is remarked.

Finally, there is no substantial difference between the results of the present study and those of Sastry *et al.* [2], in spite of the difference in rapid solidification technique.

5. Discussion

This study has clearly demonstrated that it is possible to achieve a fine and homogeneous oxide dispersion in the binary alloy system Ti–Y for any initial powder particle size below 250 μm. It is however well known that a very high cooling rate ($> 10^5$ K sec^{-1}) can be expected only for very small powder particles ($< 40\,\mu$m) which are in the extreme minority among the powder particles obtained by REP atomization. According to calculations of the solid–liquid interface

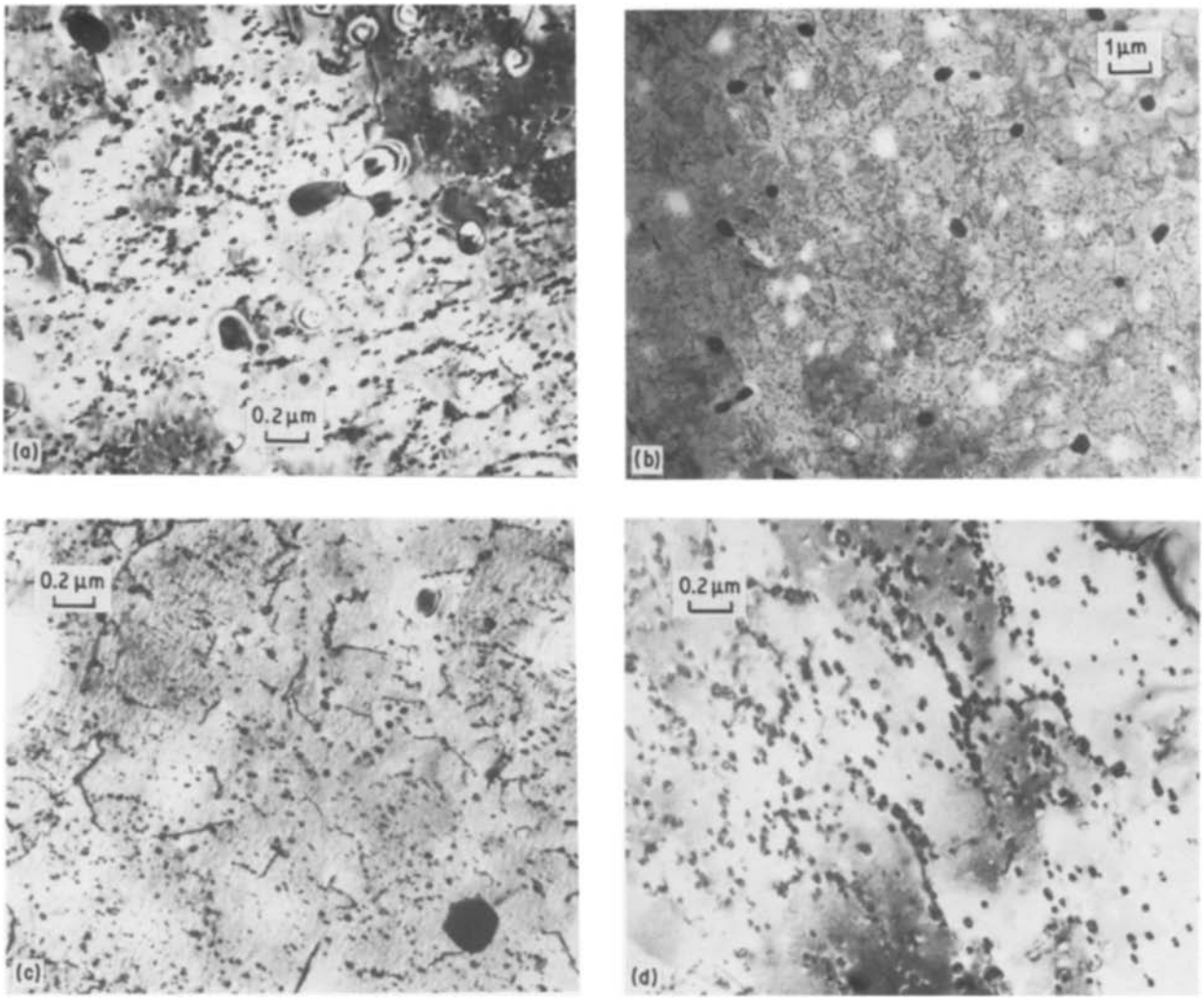

Figure 7 Fine and homogeneous oxide dispersion observed in the products consolidated by HIP at 800° C. Initial powder particle size: (a) $\phi < 40\,\mu m$, (b, c) $125 < \phi < 160\,\mu m$, (d) $200 < \phi < 250\,\mu m$. Note clear evidence of the two populations of precipitates in (b)-1.

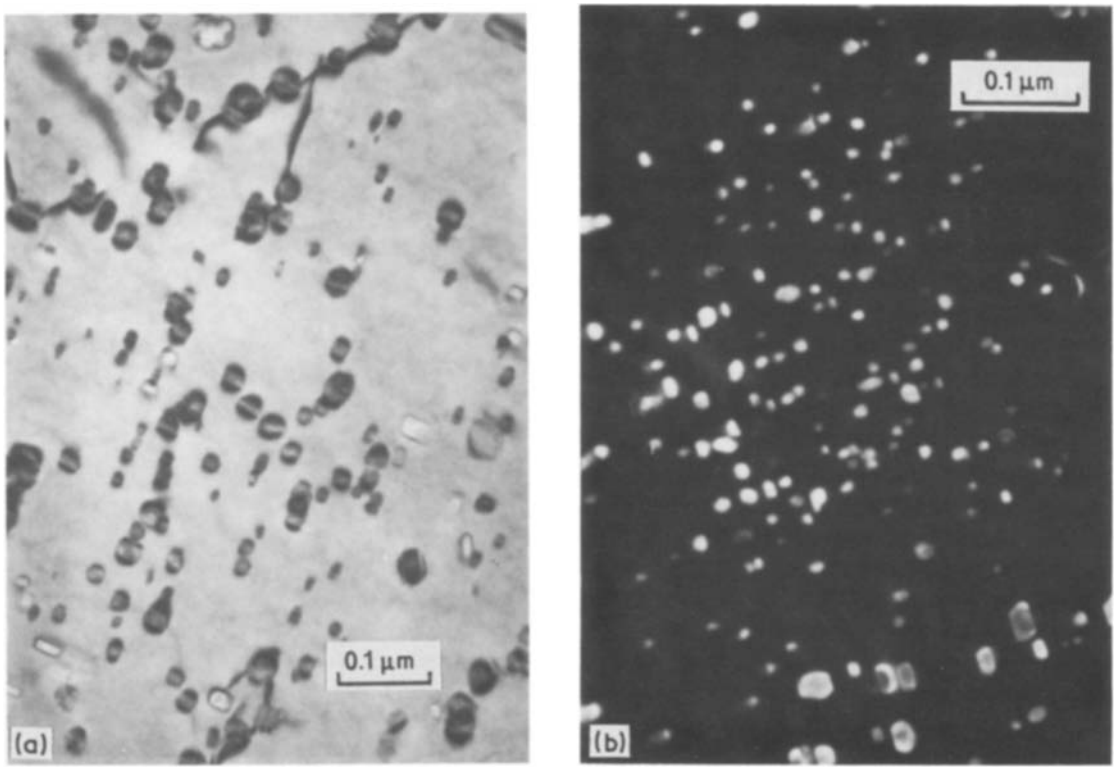

Figure 8 (a) Bright-field image of the first population of precipitates. Note a contrast due to the lattice distortion of the matrix around these precipitates. (b) Dark-field image of the first population of precipitates.

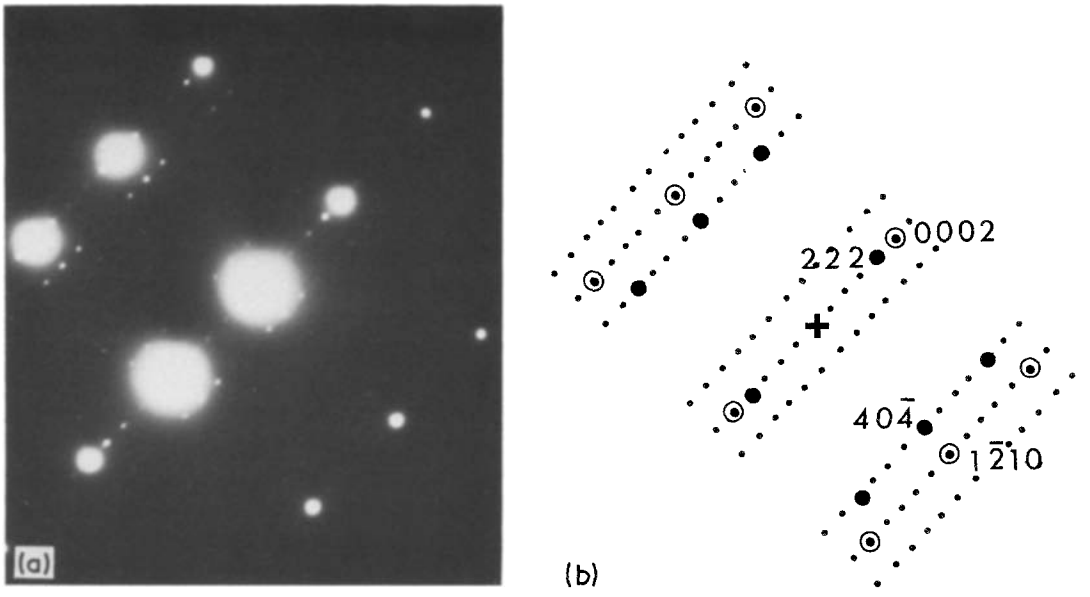

Figure 9 Selected-area diffraction pattern. (a) Diffraction pattern obtained with the beam direction parallel to $[1\,0\,\bar{1}\,0]_{Ti}$ and $[1\,\bar{2}\,1]_{Y_2O_3}$. (b) Schematic diagram. (●) reflections from Y_2O_3, (⊙) reflections from titanium (•) double diffraction spots.

velocity V_{S-L} in droplets during REP atomization, carried out on the basis of a Newtonian model, $V_{S-L} \simeq 1\,cm\,sec^{-1}$ can be expected for titanium droplets with a diameter of 250 μm, $V_{S-L} \simeq 2\,cm\,sec^{-1}$ for 100 μm, and $V_{S-L} \simeq 3\,cm\,sec^{-1}$ for 50 μm. The average cooling rate $\dot{T}$ may be related to V_{S-L} by $\dot{T} \propto V_{S-L}\Delta T/d$, where ΔT is the interval of solidification and d is the droplet diameter. If we assume $\dot{T} \simeq 10^5\,K\,sec^{-1}$ for $d = 50\,\mu m$, we obtain $3.3 \times 10^4\,K\,sec^{-1}$ for $d = 100\,\mu m$ and $7 \times 10^3\,K\,sec^{-1}$ for 250 μm. This rough calculation indicates that a great majority of powder particles (100 to 250 μm) were produced with relatively moderate cooling rates ($\sim 10^4\,K\,sec^{-1}$).

The present results of microstructural examination are essentially similar to those obtained by Konitzer *et al.* [6] on laser surface melted Ti–Er alloy: existence of the two populations of precipitates, dispersion morphology, nature of the first population precipitates. However, there are two points which must be noticed. Firstly, Konitzer *et al.* observed, regarding to the first population of small precipitates, two types of orientation relationship between precipitates and the matrix: $\{1\,1\,1\}_{Er_2O_3} \| (0\,0\,0\,1)_{Ti}$ and $\langle 1\,\bar{1}\,0\rangle_{Er_2O_3} \| \langle 1\,1\,\bar{2}\,0\rangle_{Ti}$ for the first type, and $\{1\,\bar{1}\,0\}_{Er_2O_3} \| (0\,0\,0\,1)_{Ti}$ and $\langle 1\,1\,1\rangle_{Er_2O_3} \| \langle 1\,1\,\bar{2}\,0\rangle_{Ti}$ for the second type. The first relationship was verified in the present study, but the second one could not yet be confirmed. It is not likely that the difference in oxide nature, Er_2O_3 or Y_2O_3, may explain this situation, since the various physicochemical properties of these two oxides are very similar. It is worth noting here that the second orientation relationship gives six variants, reducing radically the intensity of reflections under a selected-area diffraction condition and making its identification very difficult.

The second important point is concerned with the origin of the coexistence of the two populations of precipitate (fine and coarse) of the same chemical nature. Indeed, electron diffraction analysis on the second population of coarse precipitates suggested

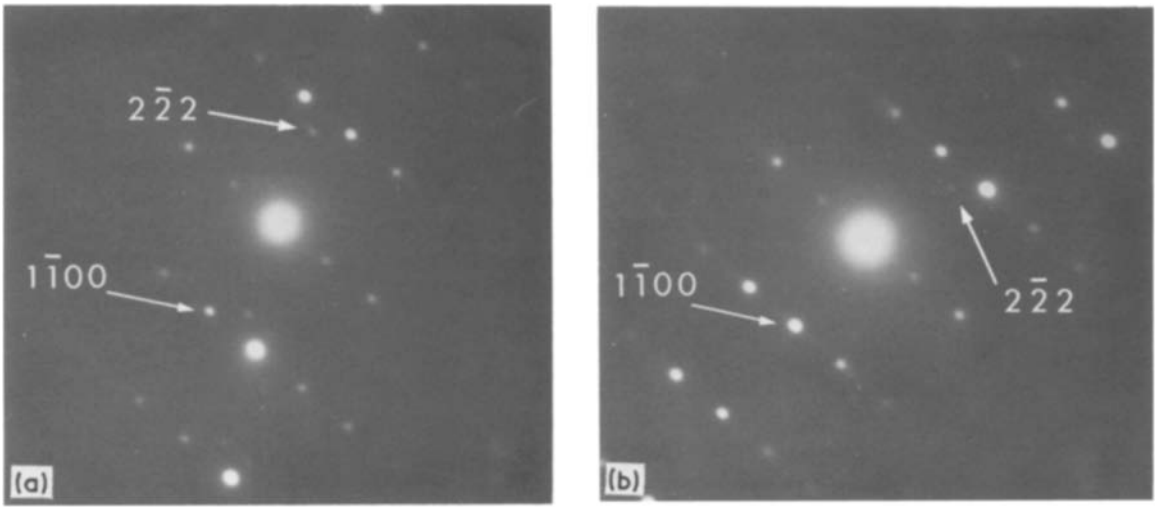

Figure 10 Diffraction patterns obtained from two selected areas slightly apart one from another in the same matrix grain. Beam direction parallel to $[1\,1\,\bar{2}\,0]$. Remark the positions of the $2\,\bar{2}\,2$ reflection of Y_2O_3 in (a) and (b).

that these precipitates were identical to the first population, i.e. Y_2O_3, although no chemical analysis was performed on these precipitates in the present study. If the present assessment is correct, then it is reasonable to assume that these two populations were not formed simultaneously. The coarse precipitates may have formed during solidification. This population probably owes its origin to the interdendritic segregation observed on a powder particle scale. It may be noticed that a certain alignment was sometimes observed on thin foils of individual powder particle for these coarse precipitates. On the contrary, the small precipitates have obviously formed in the solid state during the cooling after solidification or during hot consolidation. This is the reason why the fine dispersion was not observed systematically on all the powder particles observed before consolidation.

From the viewpoint of titanium alloy development, the sudden acceleration in the coarsening kinetics of yttrium oxide particles in the β phase field demonstrated in this study is a severe handicap for the future development of more complex alloys containing rare earth oxide dispersions. According to Konitzer *et al.* [4, 5], who predicted theoretically this inconvenient situation especially in titanium containing a rare earth element in excess after a formation of R_2O_3 (R: rare earth element), it is possible to reduce the coarsening rate to some extent even in the β phase field in the case of titanium–rare earth alloy containing oxygen in excess. The two alloys examined in this study correspond to the former case (regarding the Ti–0.74 % Y alloy, the content of yttrium was slightly in excess). It may then be interesting to examine the coarsening behaviours of yttrium oxide particles in alloys corresponding to the latter case of the theoretical prediction, by reducing still more the yttrium content or rather by increasing the oxygen content. More generally speaking, the small solubility, in the matrix, of the atomic species forming the dispersed particles would be favourable to improve the stability of the dispersion. On this basis, it may also be interesting to explore the possibility of achieving, for instance, some rare earth sulphide dispersion considering the very small solubility of sulphur in titanium. However, this type of dispersion probably requires a suitable rapid solidification equipment.

As regards the mechanical properties of consolidated products, an improvement of about 100 MPa in yield stress observed up to 550° C over titanium of commercial purity is quite reasonable value as a first rough estimation with any Orowan-type dispersion hardening model. Indeed, assuming that the Orowan stress can be added to the intrinsic strength of the matrix, we may take for instance the following expression for the strength increment [8]:

$$\Delta\sigma = 0.84 \frac{M\mu\boldsymbol{b}}{2\pi(1-\nu)^{0.5}L} \ln\left(\frac{d}{r_0}\right)$$

where M is the Taylor factor ($\simeq 3$), μ is the shear modulus, $\boldsymbol{b}$ is the Burgers vector, ν is Poisson's ratio, L is the mean interparticle spacing, d is the average particle diameter intersecting the slip plane and r_0 is the cutoff radius ($\simeq 4b$). L is given by $L = [(\pi/f)^{0.5} - 2](d/2)$ and $d = (2/3)^{0.5}D$, where f is the particle volume fraction and D is the particle diameter. Numerical application assuming $f \simeq 0.01$ and $D \simeq 30$ nm for the alloy studied in the present work leads to $\Delta\sigma = 90$ MPa.

Because of the excellent stability of the oxide dispersion observed even at 850° C, the loss of hardening effect observed above 550° C cannot be explained by the coarsening of the dispersion. This loss is presumably due to an increasing contribution of grain-boundary sliding. According to Paton and Mahoney [9], grain-boundary sliding becomes significant above 550° C in the overall plasticity of some titanium alloys. It is worth noting that in the present work the decrease in yield stress was accompanied by a sudden increase

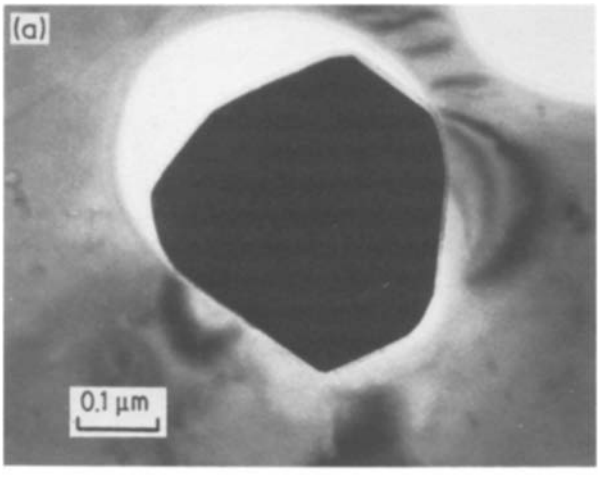

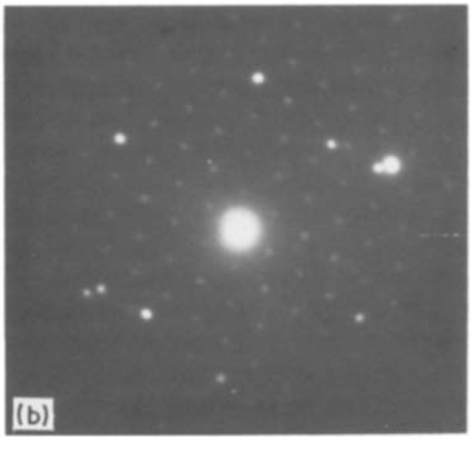

Figure 11 Example of oxide precipitates of the second population: (a) bright-field image, (b) diffraction pattern of [1 1 1] pole, (c) schematic diagram; (⊙) titanium diffraction.

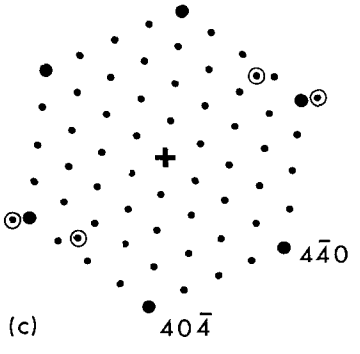

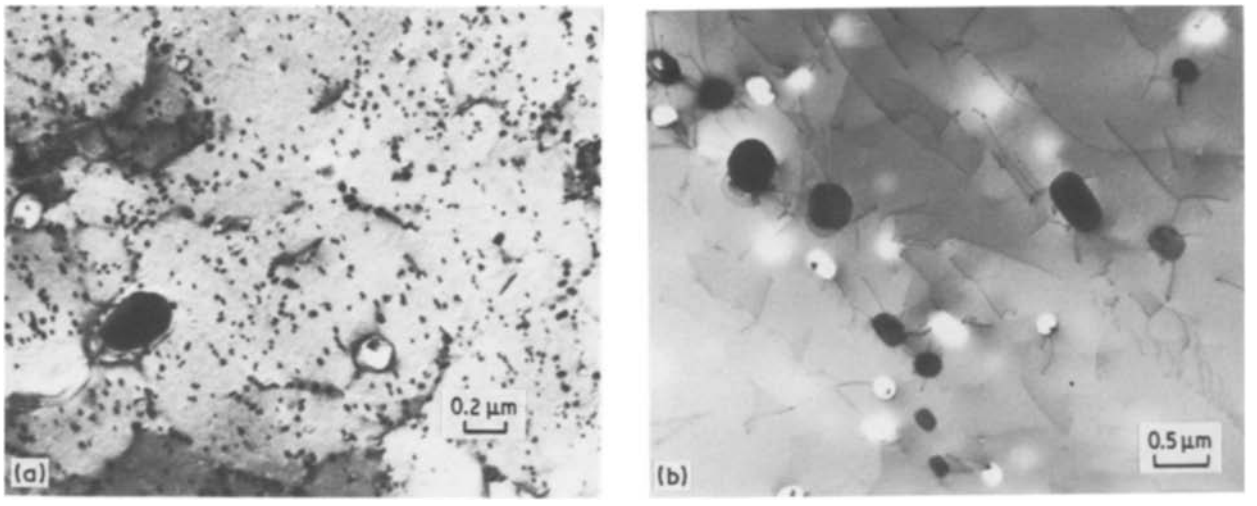

Figure 12 Influence of consolidation temperature. (a) Microstructure observed in the products consolidated at 850° C, nearly identical to those of Fig. 7. (b) Disappearance of the first population of small precipitates in the products consolidated at 920° C.

in total elongation during the tensile tests above 550° C, attaining about 100% at 700° C.

6. Conclusions

1. It is possible to achieve a fine and homogeneous dispersion of yttrium oxide, Y_2O_3, in the binary Ti–Y alloy system with relatively moderate cooling rates ($\sim 10^4$ K sec^{-1}) during solidification.

2. The stability of the oxide dispersion is excellent in the α phase temperature region, but not in the β phase region.

3. A substantial increment in strength ($\sim$ 100 MPa) is expected through yttrium oxide dispersion up to 550° C, while the improvement becomes negligible above this temperature.

Acknowledgements

This research was conducted under a contract from the French Ministry of Research and Technology. The authors would like to thank A. Lasalmonie and F. Duflos for their helpful assistance and numerous useful discussions.

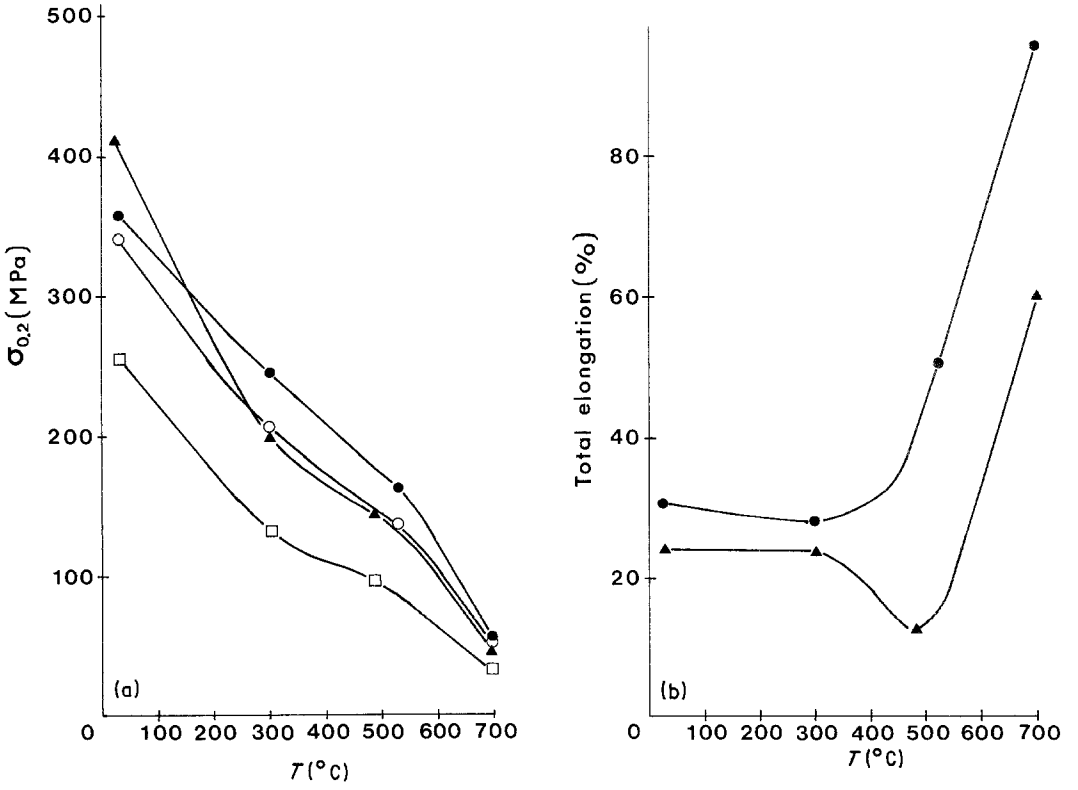

Figure 13 Temperature dependences of (a) 0.2% proof stress and (b) total elongation for (●, ○) consolidated Ti–1.84 % Y alloy with 125 < ϕ < 160 μm; (□) pure titanium; (▲) Ti–1.0 % Er (from Sastry *et al.* [2]). (●) Extruded at 800° C, (○) consolidated by HIP at 800° C.

References

1. S. M. L. SASTRY, P. J. MESCHTER and J. E. O'NEAL, *Metall. Trans. A* **15A** (1984) 1451.
2. S. M. L. SASTRY, T. C. PENG and L. P. BECKERMAN, *ibid.* **15A** (1984) 1465.
3. D. G. KONITZER, B. C. MUDDLE and H. L. FRASER, *ibid.* **14A** (1983) 1979.
4. D. G. KONITZER, B. C. MUDDLE, H. L. FRASER and R. KIRCHHEIM, "Titanium Science and Technology", Vol. I (Deutsche Gesellschaft für Metallkunde, Oberursel 1985) p. 405.
5. *Idem*, private communication, 1984.
6. D. G. KONITZER, J. T. STANLEY, M. H. LORETTO and H. L. FRASER, *Acta Metall.* **34** (1986) 1269.
7. L. EYRING, "Handbook on the Physics and Chemistry of Rare Earth", Vol. 3 (North-Holland, Amsterdam, 1979) p. 337.
8. L. M. BROWN and R. K. HAM, in "Strengthening Methods in Crystals", edited by A. Kelly and R. B. Nicholson (Applied Science, 1971) p. 9.
9. N. E. PATON and M. W. MAHONEY, *Metall. Trans. A* **7A** (1976) 1685.

Received 15 April
and accepted 30 June 1986